Ellis, R. T., J. Blaes, and L. Anderson, 2015: Orographically induced cirrus clouds in the lee of the southern Appalachian Mountains. *J. Operational Meteor.*, **3** (10), 104–123, doi: http://dx.doi.org/10.15191/nwajom.2015.0310.

Journal of Operational Meteorology
Article

Orographically Induced Cirrus Clouds in the Lee of the Southern Appalachian Mountains

RYAN ELLIS and JONATHAN BLAES
NOAA/NWS, Raleigh, North Carolina

LINDSEY ANDERSON
North Carolina State University, Raleigh, North Carolina

(Manuscript received 9 January 2015; review completed 23 June 2015)

ABSTRACT

The development of orographically induced cirrus clouds in the lee of the southern Appalachian Mountain chain can result in areas of unanticipated cloudiness downstream of the higher terrain across the Carolinas and Virginia. Both the degree of cloudiness and its impact on surface temperatures can reduce forecast accuracy. The general environmental conditions favorable for orographic cirrus development are known and have been qualitatively documented but to this point have not been extensively quantified. This study attempts to quantify the conditions necessary for orographic cirrus development across the southern Appalachian Mountains. *Geostationary Operational Environmental Satellite* imagery and atmospheric soundings are evaluated in order to better understand the most important environmental conditions needed for an orographic cirrus event to occur as well as which scenarios may produce null events. Case studies will be presented illustrating classic orographic cirrus events and their impacts on local forecast variables. Finally, best practices for operational forecasting of orographic cirrus are proposed, and the role of high-resolution models in the detection of orographic cirrus events is discussed.

1. Introduction

a. Background

The role of orography in producing mountain waves and associated cloud formations has been studied for quite some time. Some of the earliest photographs of mountain-wave clouds were presented in Henry (1899). Lindsay (1962) showed the favorable synoptic pattern for midlevel mountain-wave cloud development in the Appalachians was a low-pressure system over the northeastern United States with a trailing cold front to the east of the study area. The work focused on midlevel wave clouds in the range of 1.2–3.6 km above ground level and revealed that mountain-wave clouds were most likely to form at altitudes where the Scorer parameter (Scorer 1949) was maximized. The Scorer parameter (l^2) states that $l^2 = g\beta/U^2$, where U is the wind speed (horizontal wind component normal to the ridge), β is the Brunt-Väisälä frequency, and g the acceleration of gravity. If waves are possible, l^2 should decrease with height. This occurs when stability decreases with height, velocity increases with height, or both. The parameter is maximized at the level of greatest stability, which corresponds to the level of maximum wave amplitude and the height of cloud formation if sufficient moisture is present. It was noted that there could be multiple levels where the Scorer parameter is maximized (and sufficient moisture exists), and thus it is possible to have wave cloud formation at multiple levels simultaneously.

Conover (1964) used Television Infrared Observation Satellite (TIROS) to outline and categorize orographically induced cirrus clouds. Although most orographically induced clouds were cumuliform in nature, one category labeled "fibrous plumes" contained middle or high clouds composed predominantly of ice crystals and reported as cirrus. The environment surrounding these cloud formations was dry adiabatic from below cloud level to the tropopause. Winds were strong at middle and high levels and were unidirectional but increasing in speed with height. Brown (1983) also used the TIROS satellites, as well as aircraft, to observe mountain

Corresponding author address: Ryan Ellis, 1005 Capability Drive, Suite 300, Raleigh, NC 27606-5226
E-mail: Ryan.Ellis@noaa.gov

waves and their momentum flux over the British Isles. Visible and infrared satellite images from the TIROS-N satellite clearly depicted orographic cirrus initiating over northern England.

In the northeastern United States, three cases of orographic cirrus were observed and documented over Mount Washington, New Hampshire (Parke 1980). This study concluded that the occurrence of orographic cirrus required an atmosphere favorable for the formation of standing mountain waves with winds orthogonal to the mountain range and at least 13 m s^{-1} at mountaintop level. In addition, wind profiles showed increasing wind speed with height near the mountaintop level with a strong, steady flow at high altitudes up to the tropopause. In all three cases, an inversion or stable layer existed below 600 hPa.

The physical characteristics of orographic cirrus along the Appalachian Mountains and their associated environment are outlined extensively in a United States Department of Commerce Satellite Applications Information Note (Ellrod 1983) and are the basis for this research. The work by Ellrod found that orographic cirrus events tended to form at night and dissipated the following afternoon. Orographic cloudiness was noted often to be multi-layered, and cloud bases were typically 3.0–4.5 km above ground level with tops in the 7.5–9.0 km range. This suggests that cirrus was not the only cloud type present in many of these mountain-wave events. Orographic cirrus environments included an inversion or isothermal layer above the mountaintop level with unidirectional west or northwest winds at 18 m s^{-1} at the 700-hPa level. Wind speeds either remained steady or increased with height up to the tropopause.

Orographic cirrus events also have been observed in the western United States. Jiang and Doyle (2006) used satellite observations and simulations to examine two cirrus plume events over the Sierra Nevada ridge and the southern Rocky Mountains. Images from the Moderate Resolution Imaging Spectroradiometer (MODIS) and *Geostationary Operational Environmental Satellite* (*GOES*) were used to highlight plumes of cirrus clouds resulting from orographic lifting. Jiang and Doyle concluded that a sufficient amount of moisture in the upper troposphere (with high relative humidity and low temperatures) is necessary for orographic cirrus events to occur. Unidirectional winds with height and a strong flow above a topographical feature supportive of inertia-gravity waves were also necessary. Grubišić and Billings (2008) conducted a two-year study of mountain-wave events in the Sierra Nevada Mountains. They found that mountain-wave events tended to favor the cool season and a flow oriented orthogonally to the mountain ridge.

Analytical theory behind orographic cirrus events and mountain waves is extensive. Durran and Klemp (1983) used a two-dimensional, nonlinear, nonhydrostatic model to calculate moist airflow in mountainous terrain (Fig. 1). This model was able to reasonably reproduce analytic solutions in a two-dimensional, non-hydrostatic, compressible model. Later, Durran (1986) showed that low-level inversions were important for the development of downslope windstorms and downstream gravity wave-breaking in the upper troposphere.

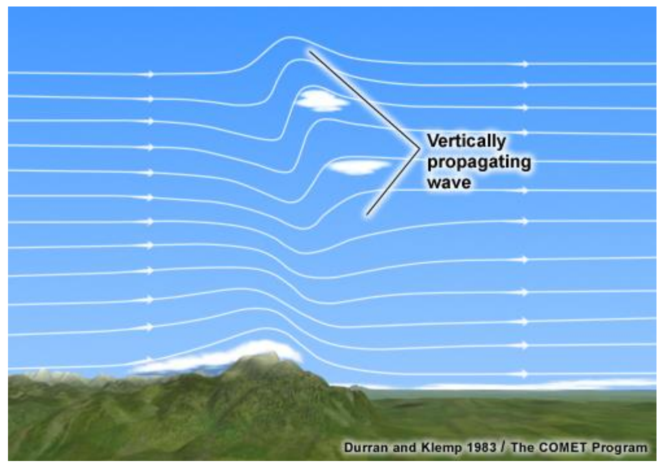

Figure 1. Schematic diagram of the airflow of a vertically propagating wave from Durran and Klemp (1983) and the COMET Program. *Click image for an external version; this applies to all figures hereafter.*

Jiang and Doyle (2008) used the Coupled Ocean/Atmosphere Mesoscale Prediction System model to look into the diurnal variation of mountain waves and wave drag associated with the flow past mesoscale ridges. It was suggested that gravity waves could be significantly stronger during the nighttime than during the daytime, even though surface winds are typically weaker at night. This is because a stable nighttime boundary layer can increase the drag needed to create mountain waves to several times the corresponding free-slip drag when the Froude number is near one (Jiang and Doyle 2008). The Froude number is defined as the nondimensional ratio of the internal force to the force of gravity for a given fluid flow. The Glossary of Meteorology [American Meteorological Society (AMS) 2015] provides the following definition (although for consistency in this paper, we use β instead of N to denote the Brunt-Väisälä frequency):

"For continuously stratified, nonrotating, dry, inviscid 2D flow over an obstacle of height h, with incoming wind speed U, and upstream Brunt-Väisälä frequency β, the quantity $U/(\beta h)$ yields a measure of whether there will be an upstream-propagating region of decelerated flow and, hence, is also sometimes referred to as the Froude number. For $U/(\beta h)>>1$, the flow ascends over the obstacle with no upstream deceleration. For $U/(\beta h)<<1$, a region of upstream flow deceleration forms that may propagate continuously upstream with time."

The dynamical influences on the cirrus cloud formation process were discussed in a paper by Lin et al. (1997) that compared an air parcel model with results from an observational measurement campaign conducted over Germany in 1994. The work concluded that in a sine-wave trajectory, ice crystal number concentration is related to wave amplitude in that air parcel trajectories with higher amplitudes produce relatively higher crystal concentrations.

More recent advances in computing resources have led to the development of more computationally expensive model-derived fields such as synthetic satellite imagery and simulated radar reflectivity [e.g., Chevallier et al. (2001); Chevallier and Kelly (2002); Otkin and Greenwald (2008); Bikos et al. (2012)]. Recent increases in temporal and spatial resolution of numerical weather prediction (NWP) model simulations and advances in the post-processing of the NWP output can result in simulations that realistically depict the spatial characteristics of the observed cloud features (Lee et al. 2014).

b. Motivation

The development of orographic cirrus clouds in the lee of the southern Appalachian Mountains (defined here as the Appalachians of Virginia, West Virginia, North Carolina, and South Carolina and referred to as "SAMs" in the rest of the paper) can be difficult to anticipate and thus may lead to inaccurate sky cover and temperature forecasts downstream, particularly in North Carolina, South Carolina, and Virginia. The difficulty models have in forecasting these events has been recently documented by Dean et al. (2005) who showed that Global Circulation Models (GCMs) lack the topographical resolution and microphysics needed to properly represent sub-grid scale, orographically produced gravity waves. As a result, GCMs can underrepresent cirrus production over continental land masses by 5–10% and by as much as 25% over some mid-latitude mountain ranges.

Despite model difficulty in forecasting orographic cirrus, the general environmental conditions favorable for cirrus development are known and have been qualitatively documented but not extensively quantified [e.g., Conover (1964); Parke (1980); Ellrod (1983); Jiang and Doyle (2006)]. Even with the prior research, further documentation of orographic cirrus development east of the SAMs is needed to better forecast these types of events. This study aims to quantify the physical characteristics associated with orographic cirrus. Scenarios where environmental conditions appear favorable but no cirrus are observed are also examined in order to try to determine which physical characteristics are most important for production of orographic cirrus. Case studies are used to demonstrate an integrated approach to forecasting cirrus events that incorporates satellite imagery, synoptic pattern, and observational soundings—as well as higher resolution models and newer NWP techniques such as synthetic satellite imagery—into the forecast process.

2. Data and methods

a. Identification of orographic cirrus events

For the purpose of this study, an orographic cirrus event (or case) is defined by the continuous formation of cirrus clouds on the lee of the SAMs with a stationary northwestern edge on the lee side of the ridge. Figure 2 shows a schematic diagram highlighting some of the physical characteristics associated with an orographic cirrus event along the SAMs. In this idealized case, flow across the mountains is northwesterly and unidirectional with height from the mountaintop through the tropopause. As the flow crosses the mountain ridge, a standing wave forms on the lee side of the mountains. This provides necessary lift and also serves as the initiation point for orographically enhanced cirrus. In addition, moisture must be present within the flow for saturation to occur and cirrus clouds to form. A moisture plume (shown in the light blue color in Fig. 2) is embedded in the northwesterly flow, usually near the 500-hPa level. This plume provides the moisture source for the orographic cirrus. Sometimes, moisture enhancements (shown in dark blue in Fig. 2) embedded within the larger moisture plume are seen on water vapor images. These enhancements can vary in size and can often be

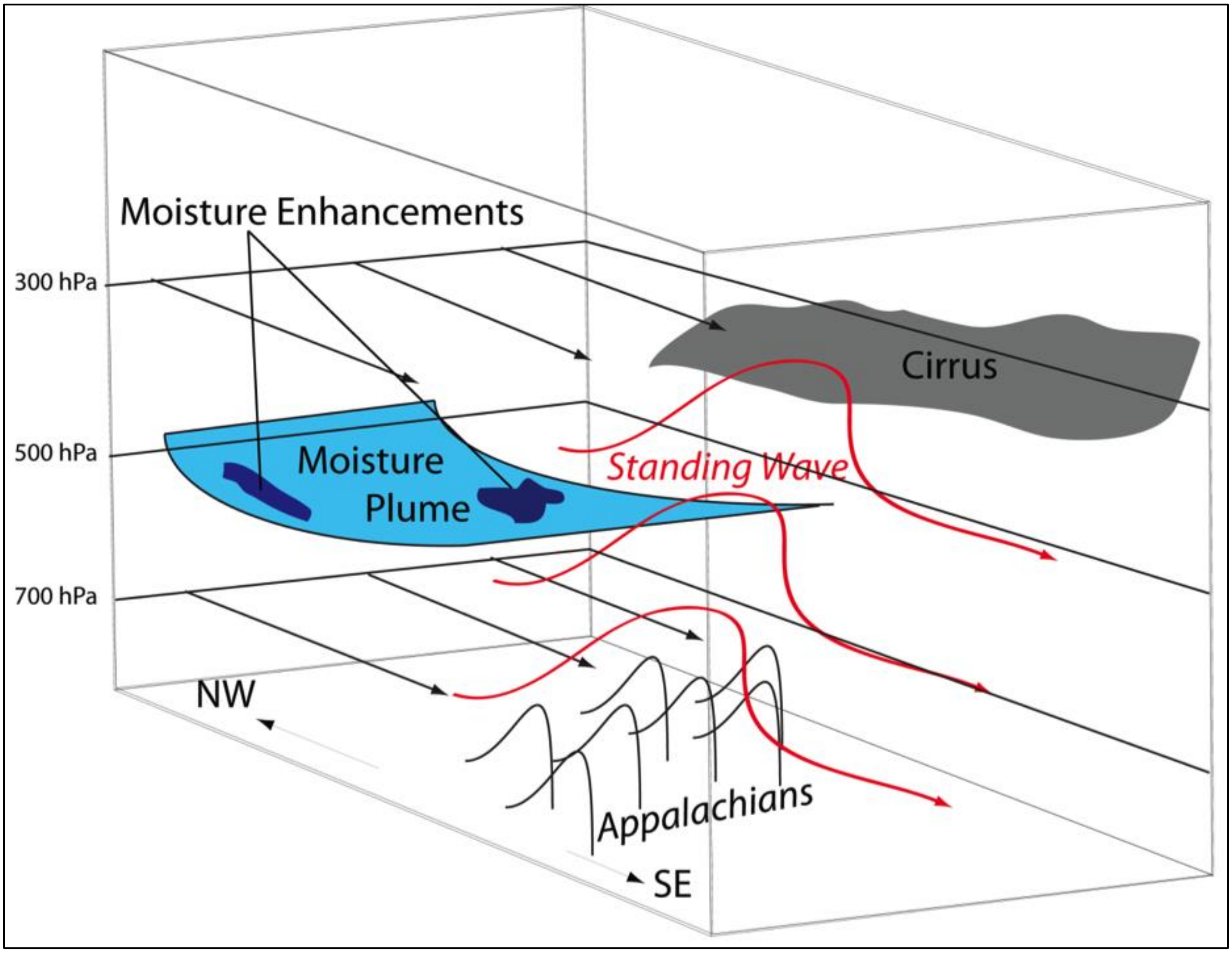

Figure 2. Schematic diagram of the physical characteristics associated with orographic cirrus development along the Appalachian Mountains with black arrows representing airflow and red streamlines representing flow over the SAMs resulting in a standing wave. Moisture enhancements (dark blue) are shown embedded in a larger moisture plume (light blue) with resulting orographic cirrus in gray.

tracked on these images. What constitutes an enhancement can best be described as a visual gradient in the water vapor images that often corresponds to a similar area of pre-existing cloud cover on the infrared images. An example of a moisture enhancement embedded within a larger moisture plume is circled in red in the first frame of Fig. 3, which shows a *GOES* water vapor (left) and *GOES* infrared (right) loop from an orographic cirrus event on 29 October 2008. Moisture enhancements within the moisture plume often serve as a catalyst for the initiation of orographic cirrus as they cross the mountains. As the moisture plume and associated enhancements cross the mountain ridge, they are lifted by the standing wave and condensation occurs in the form of orographic cirrus that is then transported downstream by the mean flow. This process continues until either the moisture source is depleted or the standing wave dissipates. Although cirrus is the cloud type most often observed with these events, midlevel clouds are often observed either along with or occasionally in place of cirrus. This is most likely due to the height of the moisture plume, the strength of the standing wave, and the vertical distance traveled before condensation occurs. In this study, all of the orographically enhanced clouds will be referred to as “orographic cirrus.”

b. 29 October 2008 case study

The 29 October 2008 orographic cirrus event is a classic orographic cirrus case in which all of the prescribed atmospheric ingredients were present over central North Carolina, but a lack of understanding of

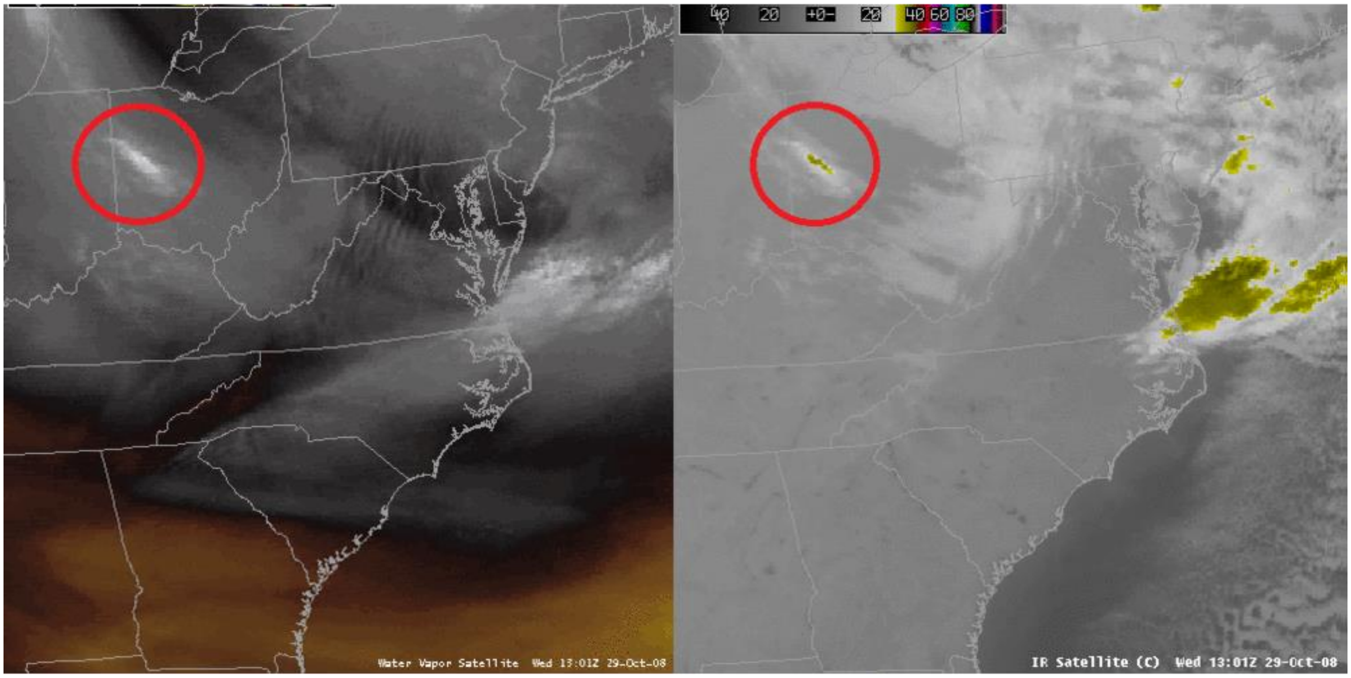

Figure 3. *GOES* water vapor image (left) and *GOES* infrared image (right) from 1301 UTC 29 October 2008 highlighting a moisture enhancement (red circle) within a larger plume of moisture prior to the onset of an orographic cirrus event east of the SAMs. *Click image for an animation from 1301 to 1745 UTC.*

the environment favorable for orographic cirrus led to an inaccurate sky cover forecast. The inaccurate sky cover forecast in turn led to an inaccurate temperature forecast. On 29 October 2008, an unforeseen shield of orographic cirrus overspread the region, hindering insolation and resulting in surface temperature differences (5–6^{o}C) between stations sheltered and unsheltered by the cirrus. This case study introduces the reader to an orographic cirrus event by examining all of the components that have been found to be characteristic of orographic cirrus. Table 1 lists all of the criteria needed for the development of orographic cirrus based on 500-hPa geopotential height analysis, atmospheric sounding data, and *GOES* water vapor imagery. Column 2 of Table 1 lists the corresponding values observed on 29 October 2008.

To assess an environment conducive for orographic cirrus, forecasters can analyze the mean upper-level synoptic pattern provided by radiosonde observations or short-term numerical models to determine whether a closer examination of satellite products and fixed sounding data is warranted before potentially adjusting the sky cover and temperature forecasts. A 500-hPa analysis for 29 October 2008 (Fig. 4) shows a negatively tilted mid-tropospheric trough over eastern Canada and the northeastern United States with a closed low pressure system over southern Quebec. A strong ridge also is present across the northern Rockies. These two features combined to create a large cyclonic circulation over much of eastern North America with a strong northwesterly flow across the Ohio Valley and SAMs.

Table 1. Listing of criteria for orographic cirrus based on atmospheric sounding, water vapor, and 500-hPa analysis data for the 29 October 2008 case study.

Criteria	**29 October 2008**
500-hPa Analysis	
Upper-level trough over northeastern CONUS with ridge to the west?	Yes
Atmospheric Sounding	
Inversion present?	Yes
Inversion in the preferred range of 850–750 hPa?	Yes (800 hPa)
Winds NW or W at tropopause?	Yes (NW)
Winds NW or W at inversion top?	Yes (NW)
Winds unidirectional or backing with height?	Yes
Wind speed increasing with height?	Yes
Water Vapor Imagery	
Upstream moisture plume?	Yes
Upstream moisture enhancement?	Yes

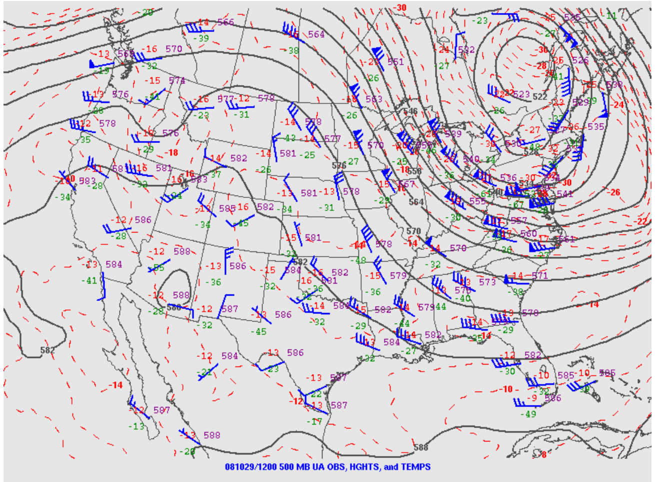

Figure 4. 500-hPa analysis from 1200 UTC 29 October 2008 (courtesy of NOAA's Storm Prediction Center).

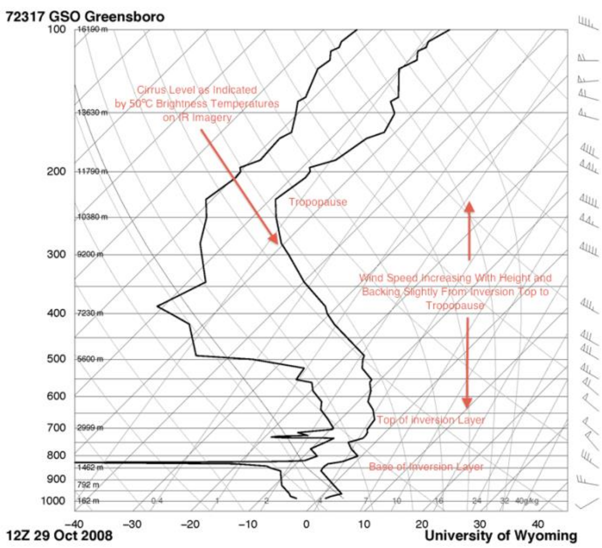

Figure 5. Skew*T*–log*P* diagram from Greensboro, NC (KGSO), from 1200 UTC 29 October 2008 (courtesy of the University of Wyoming). Key requirements for potential orographic cirrus are highlighted on the figure, as well as the level of –50°C brightness temperatures seen in Fig. 6b and Fig. 7b.

The sounding from KGSO at 1200 UTC 29 October 2008 (Fig. 5) is consistent with the six characteristics evaluated to determine if an atmospheric profile is favorable for orographic cirrus development. First, a temperature inversion was present. Second, the inversion existed near and above the mountaintop level between 850–750 hPa. At the top of the inversion and at the tropopause, the wind was from the northwest. The wind was unidirectional or slightly backing with height from the top of the temperature inversion through the tropopause. Finally, the wind speed increased from 17.5 m s^{-1} at the top of the inversion to 45 m s^{-1} at the tropopause. This sounding illustrates all the physical characteristics for orographic cirrus development and was observed a few hours prior to the onset of this particular event. One item that is inconsistent with previous studies is that this orographic cirrus event initiated during the daytime. Although we agree that most events initiate nocturnally, our research suggests that this is not as common as thought. Fig. 5 has been annotated to highlight the various characteristics favorable for orographic cirrus.

The *GOES* water vapor satellite image from 1401 UTC (Fig. 6a) shows a moisture plume with an embedded moisture enhancement prior to the onset of orographic cirrus east of the Appalachians of North Carolina and west of Greensboro, North Carolina (KGSO). The corresponding *GOES* infrared satellite image from the same time (Fig. 6b) shows pre-existing cloud cover in the location of the moisture enhancement, although the rest of the moisture plume is not observed. Fig. 6c and Fig. 6d show subsequent *GOES* water vapor and infrared images from 1815 UTC clearly depicting a broad cirrus shield across northeastern North Carolina and southeastern Virginia. Brightness temperatures within the cirrus shield were approximately –50°C and are highlighted on the KGSO sounding in Fig. 5 to show the corresponding cloud level. These images also show the straight, back edge of the shield semi-parallel to the Appalachian ridge. This is common in orographic cirrus events, and this back edge usually remains stationary for several hours before finally advancing eastward, signaling the end of the orographic cirrus event.

Infrared satellite images combined with surface observations shown in Fig. 7 illustrate the problems that forecasters can face when dealing with an orographic cirrus event. Because this case occurred during the morning and afternoon with no precipitation expected, the primary concern of forecasters would likely be the maximum temperature forecast. Surface observations reveal that sites underneath the cirrus shield reported temperatures as much as 5.5°C cooler than locations with no cloudiness.

c. Climatology of orographic cirrus events

Twenty-three unique cases of orographic cirrus events were observed and analyzed during part one of the study, which began in March 2009 and lasted through February 2010. A second study was conducted

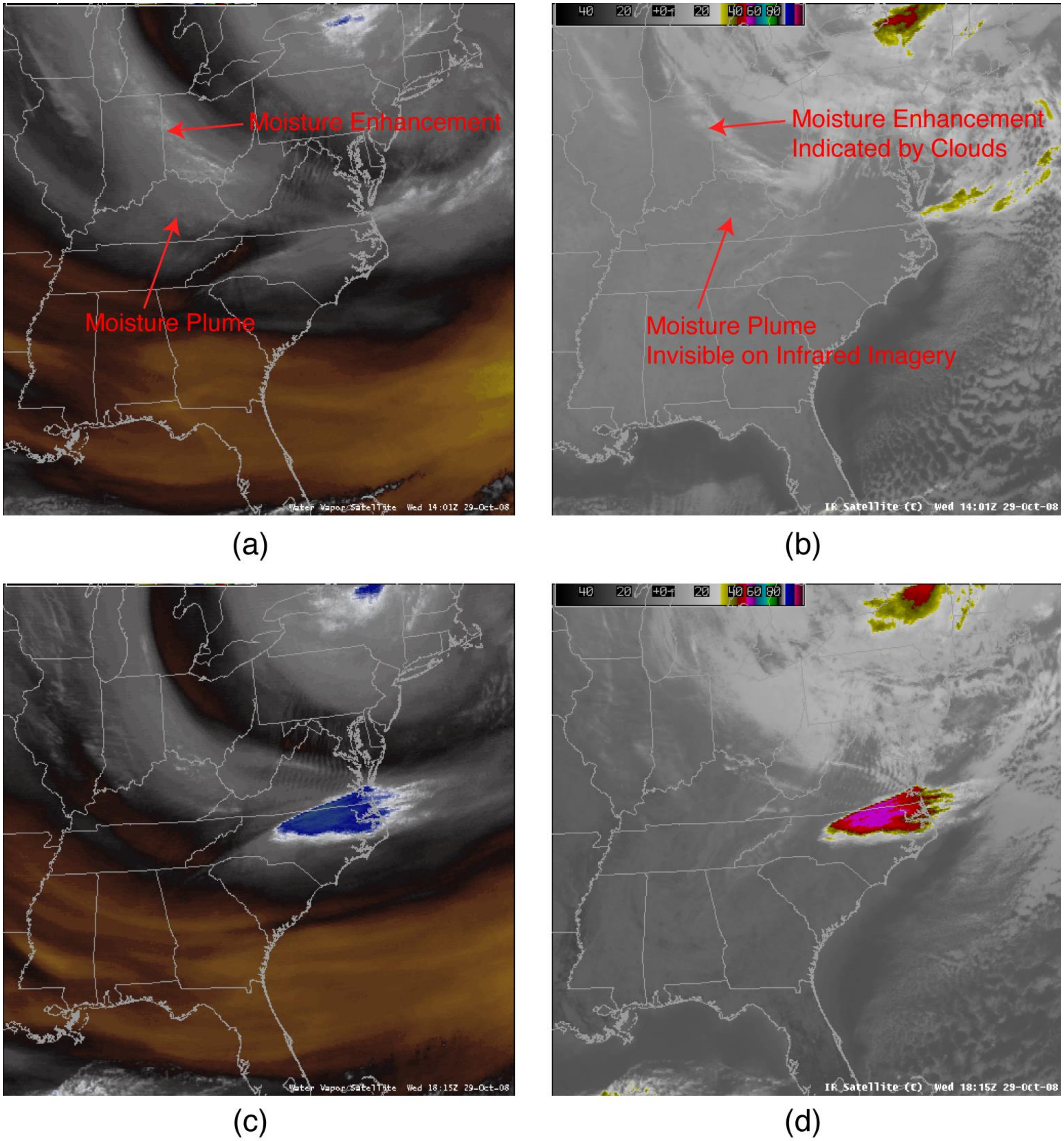

Figure 6. *GOES* (a) water vapor and (b) infrared satellite images from 1401 UTC 29 October 2008 compared with *GOES* (c) water vapor and (d) infrared satellite images from 1815 UTC 29 October 2008. The upstream moisture plume and an example of a moisture enhancement are annotated in (a) with corresponding features annotated in (b).

to target the cool season months, here defined as the months between September 2011 and April 2012. As in the 2009–2010 experiment, cirrus events were targeted. There were 42 unique orographic cirrus events evaluated and analyzed during 2011–2012, bringing the total number of orographic cirrus events analyzed for both years to 65.

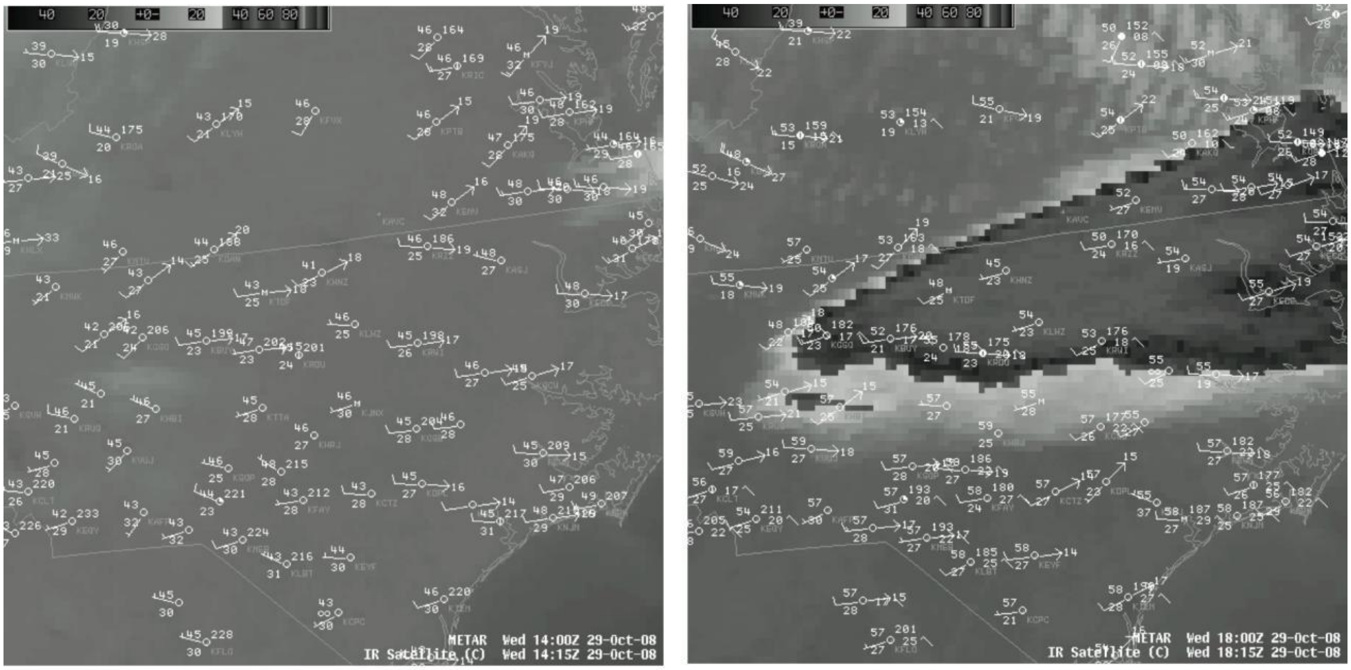

(a) (b)

Figure 7. *GOES* infrared satellite images from (a) 1415 UTC and (b) 1815 UTC 29 October 2008 with an overlay of METAR station observations. Temperatures and dewpoints depicted on surface plots are in °F.

Cirrus events were first identified by searching through *GOES* satellite data. A moisture fetch upstream of the mountain range was identified on the 6.5-µm water vapor images, which was then followed by confirmation of orographic cloud formation on the 0.65-µm visible or 10.7-µm infrared satellite images in the lee of the mountain range. Once an orographic cirrus event was identified, atmospheric soundings near the cirrus shield were collected and analyzed. Atmospheric soundings from three sites [Greensboro, North Carolina (KGSO); Roanoke, Virginia (KRNK); and Washington Dulles International Airport, Virginia (KIAD)] (Fig. 8) were analyzed to determine whether certain criteria were met indicating a favorable environment for the development of orographic cirrus in the same region as outlined in Ellrod (1983). These criteria are as follows: a temperature inversion near or above the mountaintop level, which across the SAMs would be captured in the 850–750-hPa layer; a northwesterly or westerly wind (within 30° of the cardinal direction and generally orthogonal to the Appalachian mountain chain) at both the top of the inversion and at the tropopause; wind speed increasing with height from the top of the inversion to the tropopause; and a unidirectional or backing (60° or less) wind profile with height from the top of the inversion through the tropopause. Although there were

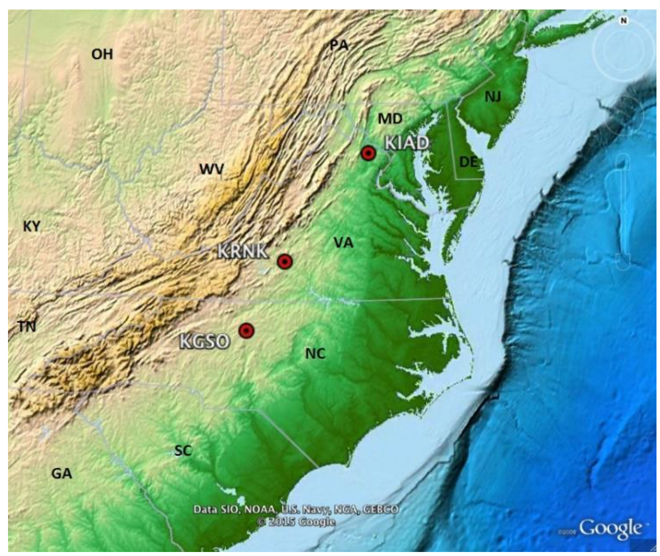

Figure 8. Shaded relief map of the eastern United States showing the three atmospheric skew*T*–log*P* locations used in this study and the location of the Appalachian Mountains. Data provided by Amante and Eakins (2009).

65 unique cirrus events, more than one atmospheric sounding may have indicated favorable conditions during the same event because of the size of the cirrus shield covering multiple sounding sites or persistence of the event lasting longer than 12 h. The total number of soundings analyzed from within cirrus environ-

ments during both the 2009–2010 and 2011–2012 studies was 123, even though there were only 65 unique cases of cirrus. Although this presents the danger of weighting certain events more than others, it is proposed that each sounding varies significantly in time and space and represents a different interpretation of what a favorable environment for orographic cirrus is and should be included in the study.

For the 65 cases of orographic cirrus, the frequency of occurrence by month was evaluated along with the onset and end times and duration of each event. The onset time for an event is defined by the first infrared satellite image where orographically enhanced cirrus is visible. For the purpose of this study, the end time for an event is defined by the time at which the stationary western edge of the cirrus shield becomes transitory and moves eastward, signaling an end to the production of orographic cirrus. It should be noted that the impacts resulting from orographic cirrus enhancement can last several hours beyond the defined end time for an event as cloud cover is transported downstream. A second set of histograms was created using all 123 soundings collected on cirrus days. This set includes the pressure level of the inversion base, pressure level of the inversion top, and depth of the inversion. Pressures were grouped into 50-hPa bins. For example, pressure values of 700–749 hPa were placed in the 700-hPa bin; pressures of 750–799 hPa were placed in the 750-hPa bin; etc.

Last, wind roses were created to show the observed wind speed and direction at the top of the inversion and at the tropopause using data from all 123 soundings collected on cirrus days. In this format, wind direction was placed in 10° bins centered on the direction in degrees. For example, wind directions of 265–274° were placed in the 270° bin. Wind speeds were placed in bins of 10 m s^{-1}. Presenting the data in this format allows for easier recognition of the most common wind direction and offers a breakdown of the frequency of a range of wind speeds at a given direction.

d. Cirrus versus non-cirrus cases

An additional analysis was done with the data collected in the 2011–2012 experiment. After satellite images were evaluated to find all instances of orographic cirrus, and soundings were collected within the cirrus environment, the remaining soundings in the cool season also were researched to find null cases (i.e., non-cirrus events). A null case is defined here as an instance where, according to the criteria presented in Ellrod (1983), the atmospheric sounding was favorable for cirrus but none occurred. Because the soundings analyzed during orographic cirrus events did not always meet all of the criteria outlined in Ellrod (1983), some flexibility was built into the analysis of potential null-case soundings. In particular, if the sounding met five out of the six criteria outlined in Ellrod (1983), it was included in the null-case analysis. This allowed for a dataset of null soundings and also null-event days, which were then compared against sounding and satellite data from the observed cases to identify the differences.

The number of null soundings found during the 2011–2012 cool season was 343. Characteristics of the null soundings were compared to soundings collected during observed events and included the inversion height, wind direction at the top of the inversion and the tropopause, a unidirectional or slightly backing wind profile, and wind speeds increasing with height between the top of the inversion and the tropopause.

After sounding data were compiled, water vapor images on the null-sounding days were examined to determine whether a moisture plume was present upstream of the SAMs, and also if there were any qualitative visual enhancements in the moisture field. During this process, satellite images were subjectively analyzed to look for pockets of enhanced moisture within the upstream moisture plume on a course to intersect the Appalachian range. A 500-hPa analysis then was used to evaluate the synoptic pattern on the null-case days.

e. NCEP/NCAR reanalysis

NCEP/NCAR reanalysis data (Kalnay et al. 1996) were gathered for each day when orographic cirrus occurred during both the 2009–2010 and 2011–2012 experiments. Reanalysis data were compiled from days when cirrus occurred and compared against data collected on days when soundings indicated a favorable environment for cirrus based on Ellrod (1983) but none occurred during the 2011–2012 cool season (i.e., non-cirrus cases). This included 65 cirrus days compared against 142 non-cirrus days. Composites were created by averaging each variable at the synoptic times (0000, 0600, 1200, and 1800 UTC) over the days specified for analysis. Composites were created for 500-hPa geopotential height, 500-hPa relative humidity, and 300-hPa vector winds for cirrus versus non-cirrus days. Anomaly fields also were created for these variables for comparison against climatological normals from 1981–2010. The 500-hPa geopotential height was used to evaluate the upper-level synoptic pattern; 500-hPa relative humidity was used to diagnose moisture aloft; and 300-hPa vector winds were obtained to analyze wind patterns at the tropopause. For more information on the process for creating composite imagery using NCEP/NCAR reanalysis data, please refer to Kalnay et al. (1996) or the National Oceanic and Atmospheric Administration (NOAA)/Earth System Research Laboratory Physical Sciences Division web site at www.esrl.noaa.gov/psd/data/gridded/reanalysis/.

3. Results

a. Physical characteristics and climatology of observed cirrus events

Combining the data from both the 2009–2010 and 2011–2012 studies yields 65 unique cases of orographic cirrus with a total of 123 atmospheric soundings analyzed within these 65 cases. Frequency histograms (Fig. 9) clearly show that orographic cirrus events are a cool-season phenomenon (Fig. 9a). December through March are shown to be the most likely months for orographic cirrus to occur, with some cases also occurring in October, November, and April. Event duration (Fig. 9b) varied from <2 to 14 h in length. Although event duration was determined with a temporal resolution of 15 min using *GOES* satellite data, it is presented on the histogram in two-hour time bins for ease of visualization.

Although Ellrod (1983) discussed these events as primarily nocturnal, data from this research indicate that, even though a nocturnal mode is more favorable for initiation, events have been documented to begin and end at various hours throughout the day if stability is present at the mountaintop level. Of the 65 cases observed, 52 (80%) initiated from a predominately nocturnal time range of 0000–1200 UTC (Fig. 9c), and 42 (65%) events ended in a generally diurnal time range of 1200–0000 UTC (Fig. 9d).

When examining the 123 atmospheric soundings collected within the cirrus environment, the observed inversion base ranged from 999 up to 600 hPa (Fig. 10a). The inversion base was found to be between 899 and 800 hPa 62% of the time. The inversion top also ranged from 999 to 650 hPa, but it was more likely found between 849 and 750 hPa (56% of the time, Fig. 10b). The depth of the inversion varied widely but was between 0 and 39 hPa 75% of the time (Fig. 10c).

Wind roses (Fig. 11) show that the dominant wind direction at the top of the inversion (Fig. 11b) was northwesterly (295–314°). This is not surprising because, in order for cirrus to initiate across the Appalachian ridge, it at least should have a westerly component with the most favorable direction being orthogonal to the mountains, which in this case is northwesterly. The most common wind speed in the northwesterly direction was a range of 10–20 m s^{-1}. This combination of wind speed and direction occurred more than 30% of the time at the inversion top. It should be noted here that, in the small number of cases where northeasterly flow was observed at the inversion height, winds more orthogonal to the ridge were observed in the sounding data just above the inversion height through the tropopause. At the tropopause, a westerly direction (265–274°) was the most common (Fig. 11a) and also occurred more than 30% of the time. The most common range of wind speeds at the tropopause was 30–40 m s^{-1}, which occurred about 10% of the time. These statistics support the finding of a slightly backing vertical wind profile with height.

b. Cirrus versus non-cirrus events

Comparisons of soundings and satellite images between cirrus and null cases (as defined in section 2d) were made for the 2011–2012 cool season (Fig. 12). There were 87 total soundings for cirrus events and 343 for null events. In the observed cirrus soundings, the temperature inversion occurred in the target range of 850–750 hPa 89% of the time as opposed to 84% of the null soundings. A northwesterly wind direction, which is most favorable for orographic cirrus events, actually occurred more frequently in null soundings at both the top of the inversion (86% for null versus 82% for observed) and at the tropopause (79% for null versus 75% for observed). Wind speed increasing with height was almost always observed in both cirrus (99%) and null soundings (98%). A unidirectional wind with height above the inversion layer was observed more frequently in the cirrus soundings (99%) versus null soundings (91%). These results suggest that favorable sounding profiles for orographic cirrus events are observed frequently in the cool season and by themselves are not sufficient to discern when a cirrus event will occur.

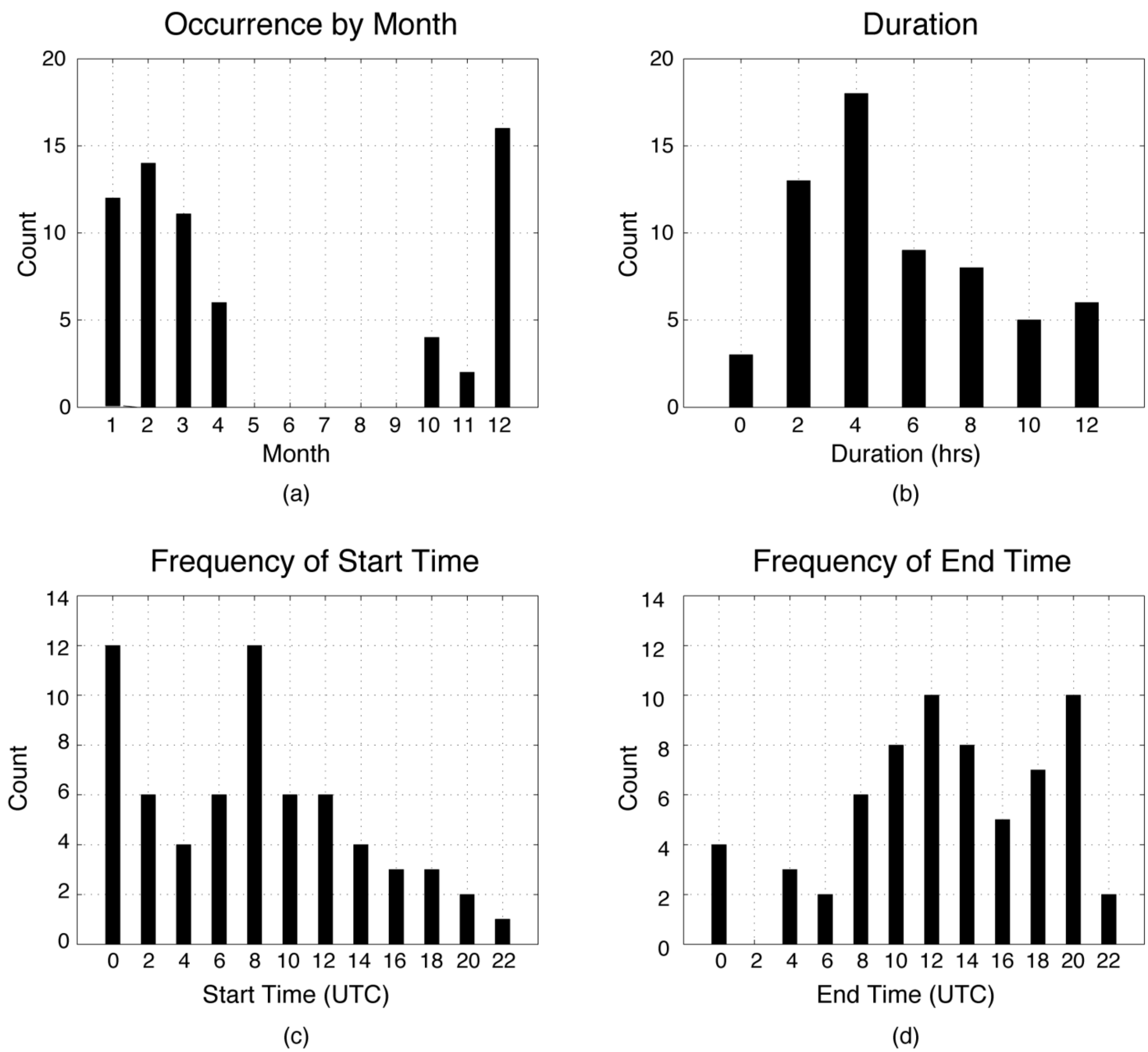

Figure 9. Frequency of orographic cirrus events by (a) month, (b) duration, (c) start time, and (d) end time.

c. NCEP/NCAR reanalysis

A comparison of NCEP/NCAR reanalysis data (Kalnay et al. 1996) was completed for days when a cirrus event occurred and those when atmospheric soundings show an environment favorable for cirrus without subsequent observation. Variables analyzed included 500-hPa geopotential height, 500-hPa relative humidity, and 300-hPa vector winds. A composite of 500-hPa geopotential height on cirrus case days (Fig. 13a) was compared to the same for non-cirrus days (Fig. 13b). The results differentiate between a favorable atmospheric profile and when cirrus will actually occur.

Even greater differences were seen in the 500-hPa geopotential height anomaly field (as compared to climatology from 1981–2010) for cirrus days (Fig. 13c) and non-cirrus case days (Fig. 13d). The 500-hPa geopotential height anomaly field for cirrus case days showed a dipole pattern with negative anomalies off the Northeast coast and positive anomalies across the Midwest, suggesting a more amplified pattern. The 500-hPa geopotential height anomaly field for non-cirrus case days showed positive anomalies across the

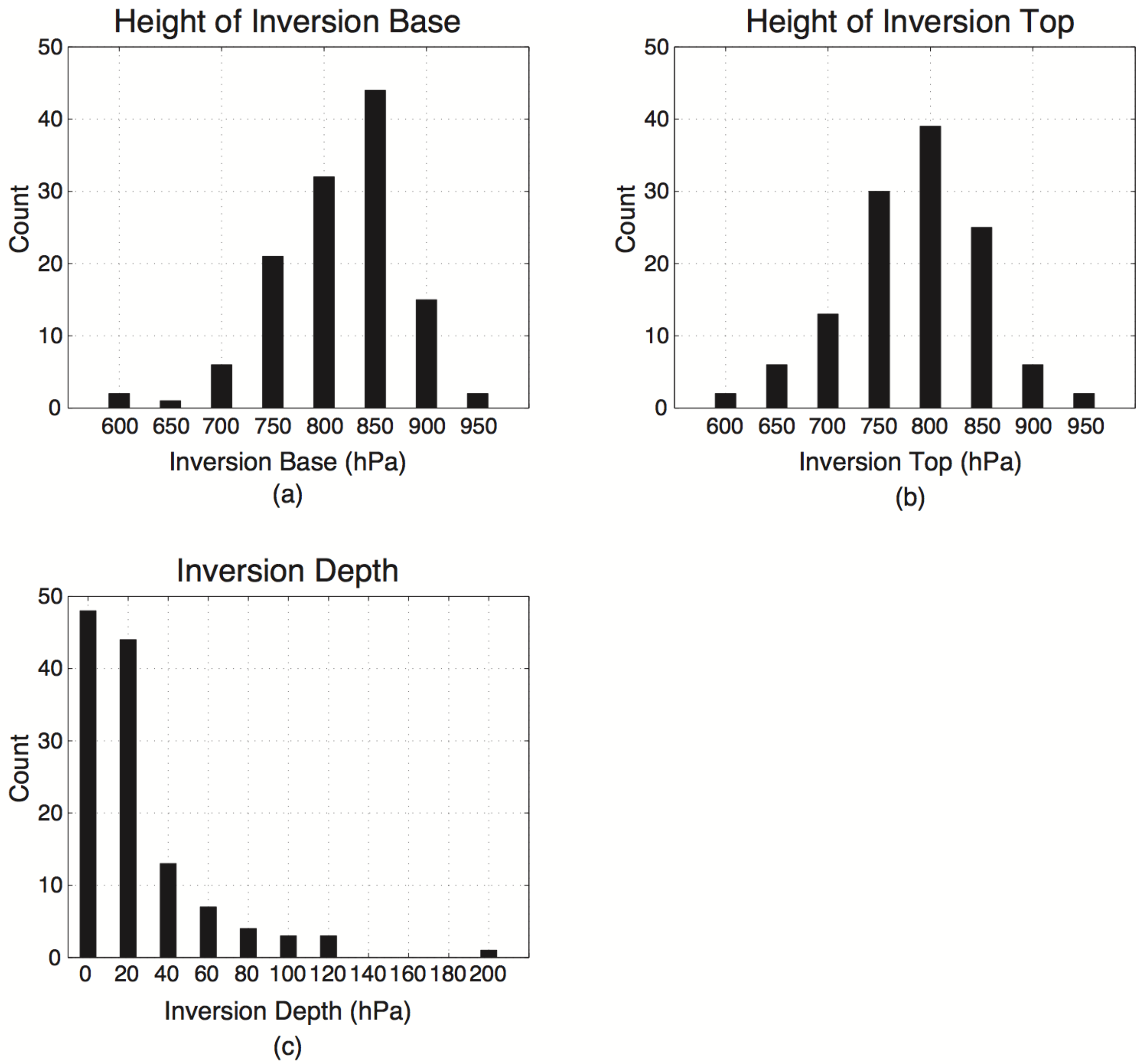

Figure 10. Histograms showing cirrus event inversion statistics including (a) inversion base, (b) top, and (c) depth.

domain with larger anomalies across the Midwest. This analysis suggests that a more amplified pattern with lower heights across the Northeast is more typical of orographic cirrus events.

Similar composite and anomaly analyses of 500-hPa relative humidity were done comparing cirrus days to non-cirrus days. For cirrus case days, the composite analysis (Fig. 14a) showed relative humidity values of 34–38% west of the SAMs. The composite analysis for non-cirrus case days (Fig. 14b) showed a subtle decrease in relative humidity values along the SAMs as compared to the cirrus case days (31–34%). Additionally, 500-hPa relative humidity anomaly fields were very similar for cirrus (Fig. 14c) and non-cirrus case days (Fig. 14d) with values of about 3–5% below normal near the Appalachian Mountains. Any differences between the two anomaly fields were insignificant.

Results for composite and anomaly analyses of 300-hPa vector winds depicted differences between cirrus case days (Fig. 15a) and non-cirrus case days (Fig. 15b). Winds at 300 hPa in the vicinity of the Appalachian Mountains averaged 35 m s^{-1} on cirrus case days and a slightly slower 32 m s^{-1} on non-cirrus

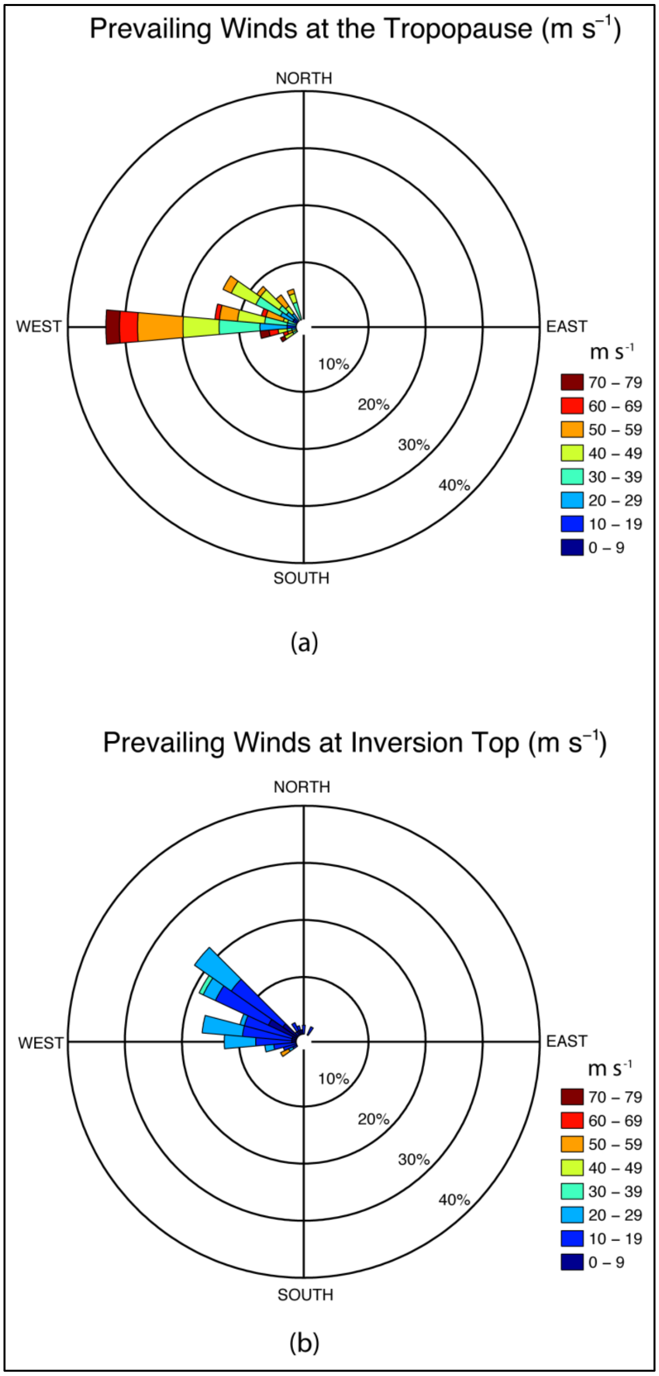

Figure 11. Wind roses for the frequency and strength of wind speed and direction at the (a) tropopause and at the (b) inversion top.

days. The jet position for the cirrus cases was farther south and more downshear than the non-cirrus cases. Anomaly fields for the 300-hPa winds demonstrated similar results, with both scenarios having an anomalous northerly component to the winds. Cirrus case days (Fig. 15c) had a larger positive anomaly at 9 m s^{-1} compared to the 5 m s^{-1} anomaly for non-cirrus days (Fig. 15d). These results are consistent with a conceptual model that the winds should be out of the west or northwest at the tropopause with faster flow on cirrus days in the proximity of a right-entrance region of an upper-level jet. The anomalous northerly component on cirrus days and the fastest winds moving out of the area further support an upper-level pattern favorable for orographic cirrus that consists of an upper-level trough axis exiting to the east with northwesterly flow behind the trough axis.

4. Conclusions and discussion

The inability to accurately anticipate orographic cirrus, including poor predictions from lower resolution NWP models, can lead to a chain reaction of erroneous forecasts starting with cloud cover and leading to deficiencies in hourly, maximum, and minimum temperature forecasts. This study aimed to identify the physical and climatological characteristics of orographic cirrus events. Although some of these have been known for some time (Ellrod 1983), quantification of these characteristics has not been thoroughly accomplished in an empirical study. A forecast strategy was developed using synoptic pattern recognition and atmospheric soundings to identify environments favorable for orographic cirrus development. Once a favorable environment was identified, water vapor images, as well as visible and infrared satellite products, were interrogated in order to identify moisture plumes orthogonal to the Appalachian ridge. Water vapor images also were used to track moisture enhancements within the plume, known to act as catalysts for the initiation of an event. Using NCAR/NCEP reanalysis data, cirrus environments were compared to seemingly favorable scenarios that did not produce orographic cirrus. Finally, new trends in high-resolution NWP models, including synthetic satellite imagery, have shown promise in forecasting the onset of orographic cirrus events.

Orographic cirrus events were found to be most common in the cool season, with December through March being the most favored months. Although previous work showed events were mostly nocturnal, this study suggests that orographic cirrus events tend to form during the overnight hours but can last into or even initiate during the daytime hours. However, the duration of the event was shown to be less predictable, and the results were not statistically significant. Examining atmospheric soundings during cirrus events

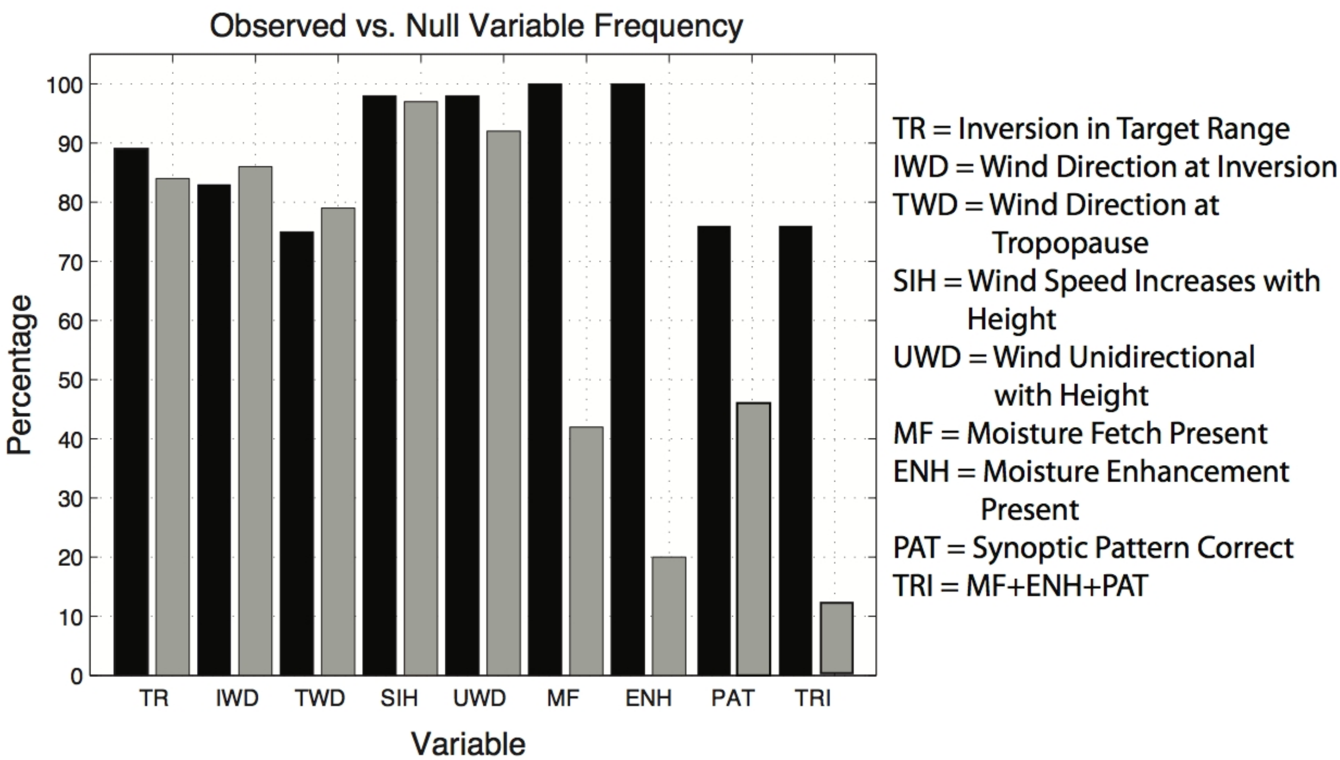

Figure 12. Observed (black) versus null (gray) variable frequency for orographic cirrus events during the 2011–2012 cool season. Each bar is represented by the variables listed to the right of the figure.

showed that a temperature inversion is usually present near mountaintop level. The wind profile tends to be unidirectional from the northwest or west with some slight backing from the top of the inversion to the tropopause. Wind speeds generally increase with height.

The synoptic pattern associated with orographic cirrus events usually consists of a mid-tropospheric trough over eastern Canada and the northeastern United States with a ridge across the northern Rockies or Plains states. These features combine to create a large cyclonic circulation over much of eastern North America with a strong northwesterly to westerly flow across the Ohio Valley and Appalachians. A pre-existing upstream moisture plume is usually necessary for a cirrus event to occur. Small enhancements within the moisture plume are often coincident with pre-existing high clouds and can signify the onset of orographic events once they cross the Appalachian range.

Atmospheric soundings, synoptic pattern, and satellite images from observed orographic cirrus cases and null cases were compared and contrasted. All of the sounding parameters favorable for orographic cirrus were observed almost equally, if not more frequently, in non-events as in cirrus cases. This was not true when considering the synoptic pattern or satellite images. Examining the synoptic pattern revealed that the proper alignment of a ridge over the Midwest, with a mid-tropospheric trough over eastern Canada and the northeastern United States, was present three-quarters of the time during the observed cases versus less than half of the time for the null soundings. Satellite data revealed that a midlevel moisture enhancement embedded within a broader moisture plume was always found upstream of an atmospheric sounding site that later experienced orographic cirrus. In non-cases, a moisture enhance-ment was only present about one-fifth of the time, making this a key discriminator between cirrus sound-ings and null soundings of orographic cirrus (Fig. 12).

In order to improve operational forecasts during potential orographic cirrus events, a forecaster can utilize a forecast funnel approach. Pattern recognition is the first step in this process. During the cool season, forecasters should look for a mid-tropospheric trough over eastern Canada and the northeastern United States with a ridge across the northern Rockies or Midwest. These two features combine to create a large cyclonic circulation with a northwesterly flow across the Ohio Valley and Appalachians. Next, the forecaster can interrogate observed atmospheric soundings in order to look for a temperature inversion near mountaintop level, a unidirectional or slightly backing northwest-

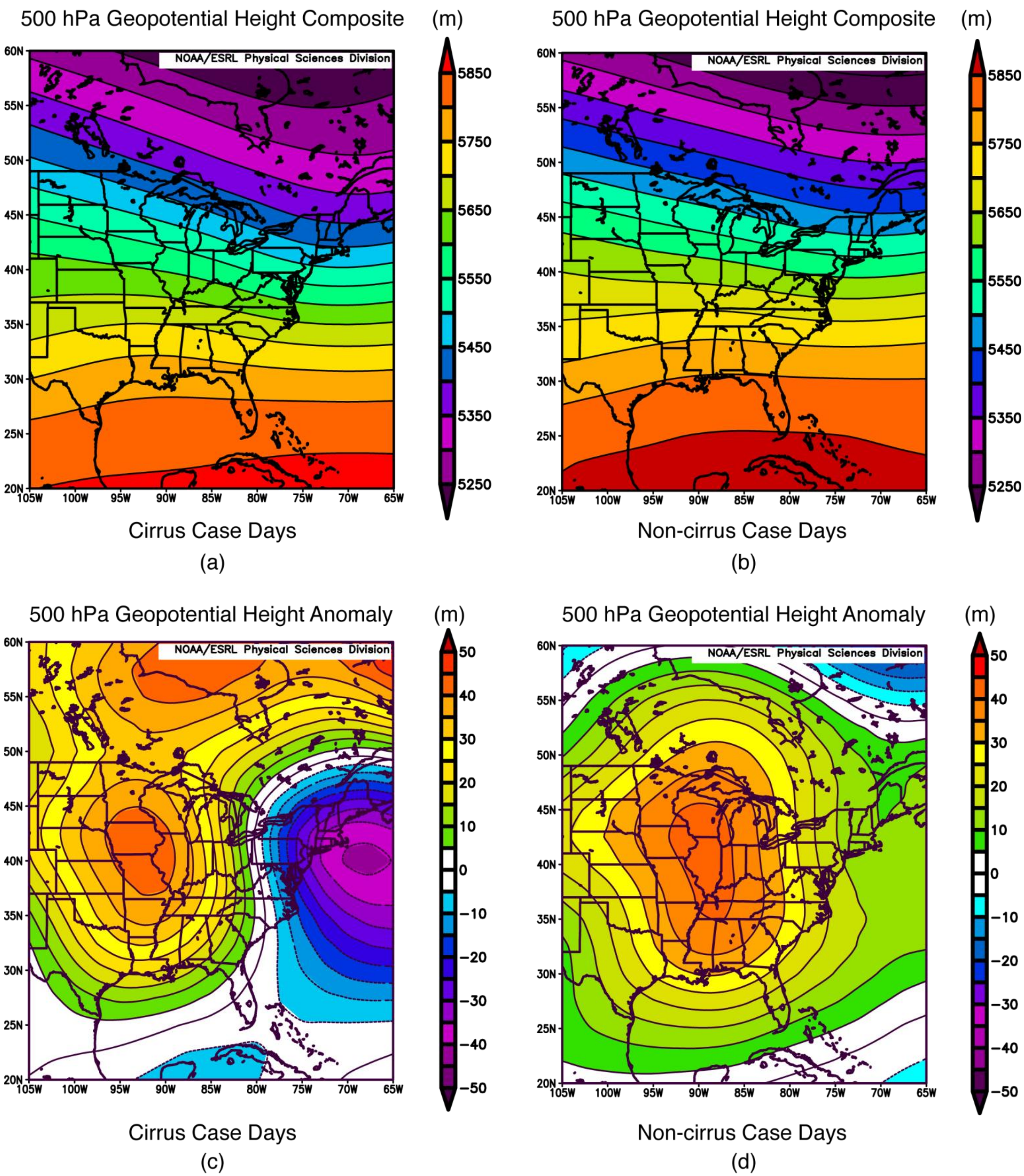

Figure 13. 500-hPa geopotential height composite of (a) cirrus days and (b) non-cirrus days from NCEP/NCAR reanalysis data and 500-hPa geopotential height anomaly field as compared to 1981–2010 climatology for (c) cirrus and (d) non-cirrus days. Image provided by the NOAA/ESRL Physical Sciences Division, Boulder, CO, from their web site at www.esrl.noaa.gov/psd/.

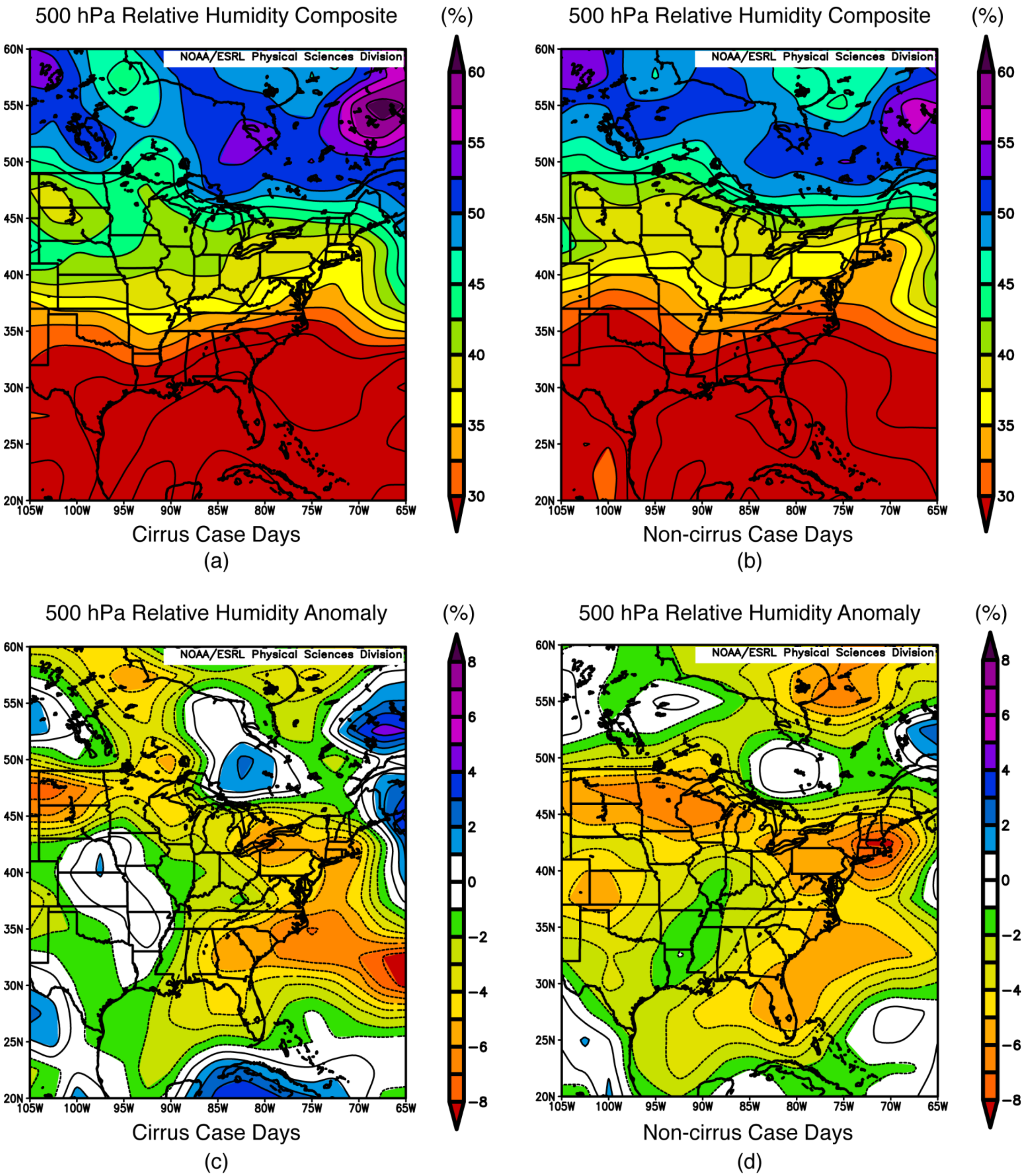

Figure 14. Same as for Fig. 13 except for relative humidity.

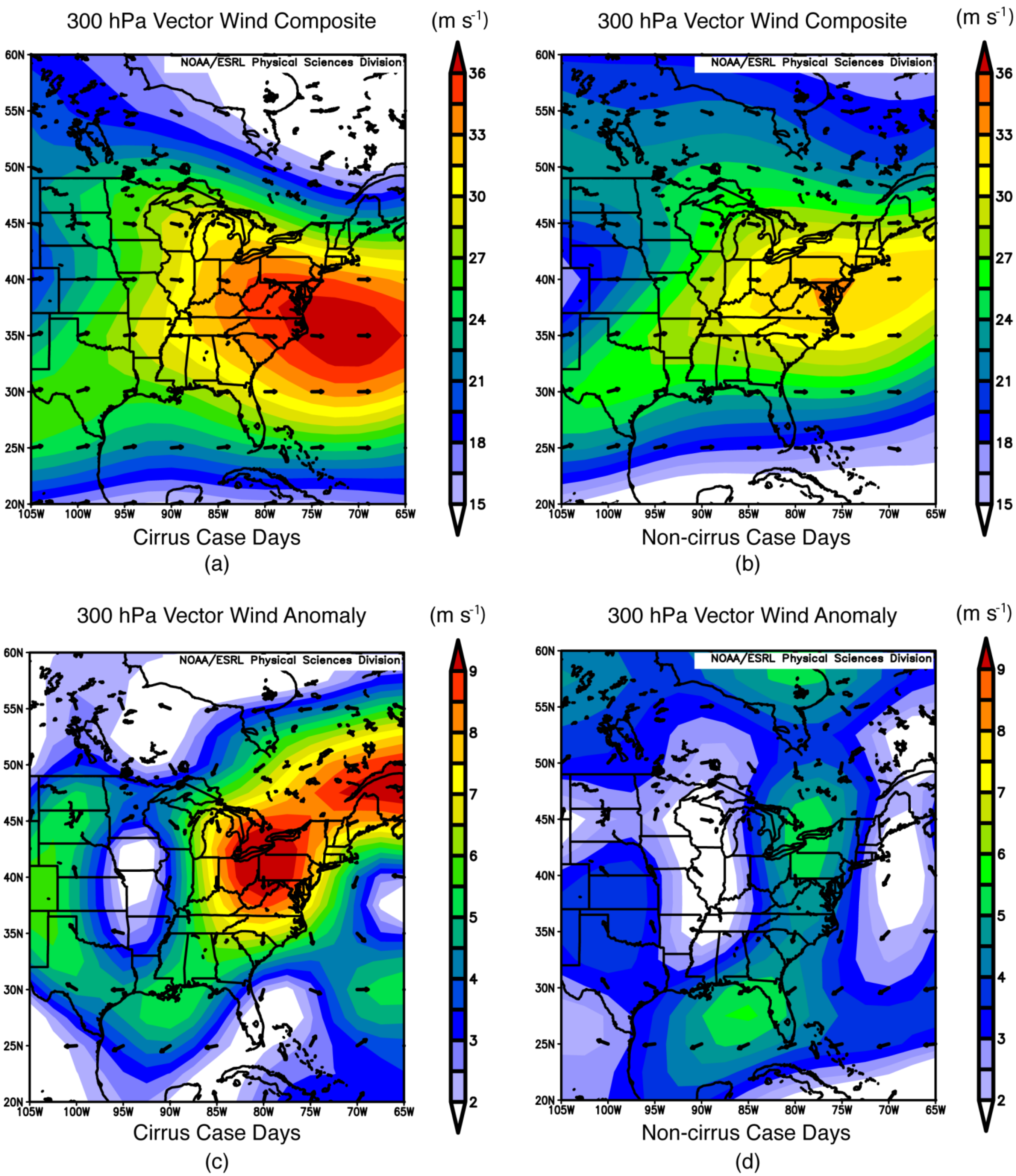

Figure 15. Same as for Fig. 13 except for 300-hPa vector wind.

erly wind profile, and wind speeds increasing with height. Water vapor imagery can then be examined to determine if there is an upstream moisture plume. Event onset can sometimes be predicted by tracking visual enhancements in the moisture field from the Ohio Valley across the Appalachian range. The trajectory of the moisture fetch will give clues as to the geographic area that will be affected by cirrus on the lee side of the mountain range. Output from high-resolution NWP models, such as synthetic satellite imagery or relative humidity fields at upper levels, could also be consulted during the forecast process to help identify and lend confidence to event timing and geographic distribution.

To demonstrate, an example orographic cirrus event from 7 January 2015 across the SAMs exhibits many of the characteristics and features noted by Ellrod (1983). The event occurred during the cool season and began during the early morning hours with an expansive shield of orographic cirrus clouds eventually extending from North Carolina across Virginia into Delaware, Maryland, and offshore. The synoptic pattern across the eastern United States was characterized by a deep-layer, long-wave trough at 500 hPa (Fig. 16). Atmospheric soundings across the SAMs noted favorable conditions for orographic cirrus with the 1200 UTC 7 January 2015 sounding from Roanoke, Virginia (KRNK), which was most representative of the orographic cirrus region (Fig. 17). The KRNK sounding depicted an inversion or isothermal temperature layer just above mountaintop height and extending from around 830 hPa to 650 hPa. The winds above mountaintop level were generally unidirectional with a slight backing with height as speeds increased from near 23 m s^{-1} at 800 hPa to more than 72 m s^{-1} at the tropopause. *GOES* water vapor and infrared images (Fig. 18a and 18b) from 0700 UTC depict the event in progress with a large moisture plume upstream of the SAMs containing a large moisture enhancement corresponding to pre-existing high clouds. The same images from 2300 UTC (Fig. 18c and 18d) show dry air replacing the moisture plume in the water vapor images and orographic cirrus ending and exiting to the east in the infrared imagery. Fig. 19 shows an animation of the observed *GOES* water vapor images from 0845 UTC to 2200 UTC on 7 January 2015.

An example loop of synthetic satellite imagery created by the Cooperative Institute for Research in the Atmosphere (CIRA) from the National Severe Storms Laboratory 4-km WRF-ARW (35 vertical levels) model initialized at 0000 UTC on 7 January 2015 is shown in Fig. 20. This animation includes the 9–22 h forecast of simulated water vapor images (6.95 µm), which is very similar but not identical to the *GOES* water vapor images (6.5 µm) shown in the previous example case. Unfortunately, the integration

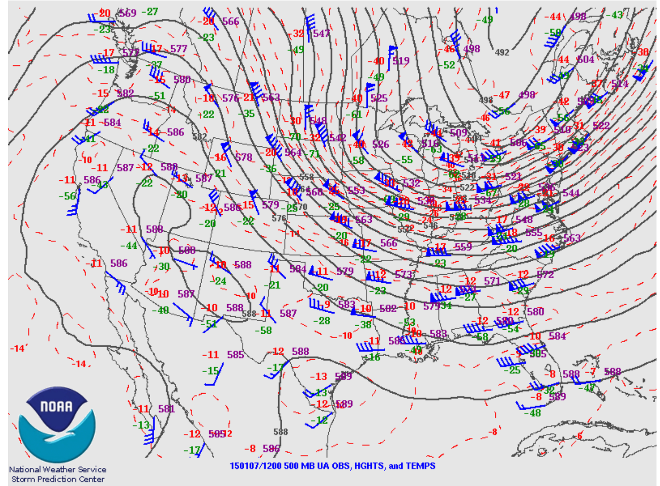

Figure 16. 500-hPa analysis from 1200 UTC 7 January 2015 (courtesy of NOAA's Storm Prediction Center).

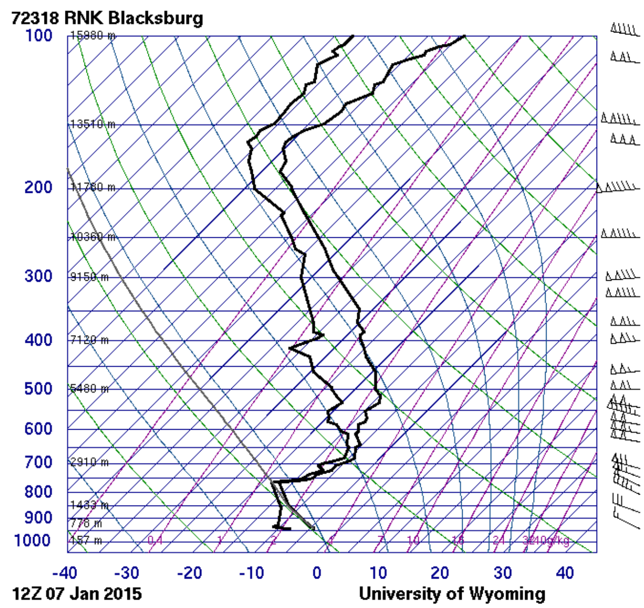

Figure 17. Skew*T*–log*P* diagram from Roanoke, VA (KRNK), from 1200 UTC 7 January 2015 (courtesy of the University of Wyoming).

of synthetic satellite imagery, such as the 6.95-µm CIRA product, into routine NWS forecast operations has been inhibited by the limited distribution and integration of these products into NWS forecast software such as the Gridded Forecast Editor (Hanson et al. 2001).

Future work on this topic will examine how higher temporal and spatial resolution imagery from the *GOES-R* Advanced Baseline Imager can be integrated into the orographic cirrus forecast process. An analysis of verification statistics of temperature and sky cover during cirrus events to quantify the effects of cirrus on

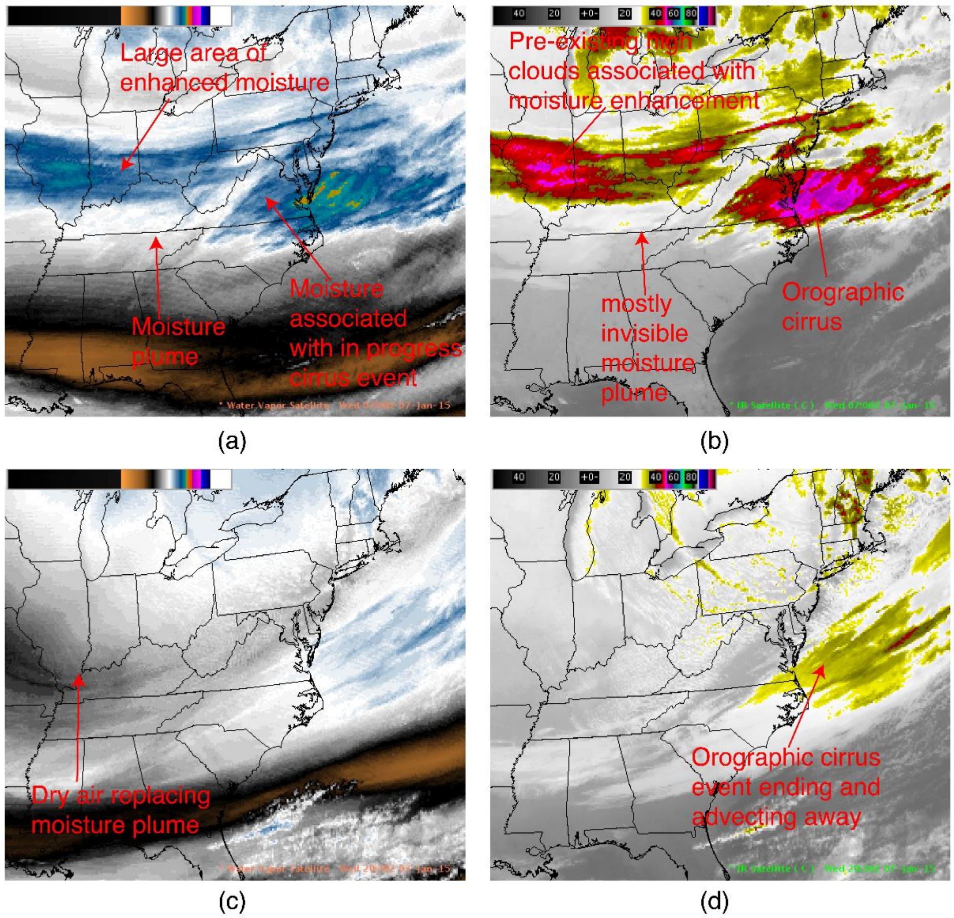

Figure 18. *GOES* (a) water vapor and (b) infrared satellite images from 0700 UTC 7 January 2015 and *GOES* (c) water vapor and (d) infrared images from 2030 UTC 7 January 2015.

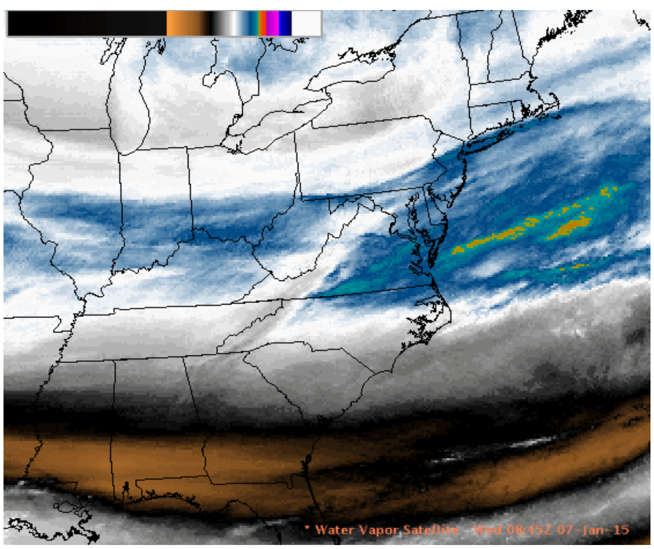

Figure 19. *GOES* water vapor image from 0845 UTC 7 January 2015. The moisture plume extending across the Missouri and Ohio Valleys becomes enhanced after crossing the SAMs, indicating upward vertical motion and increasing moisture. *Click image for an animation from 0845 to 2200 UTC.*

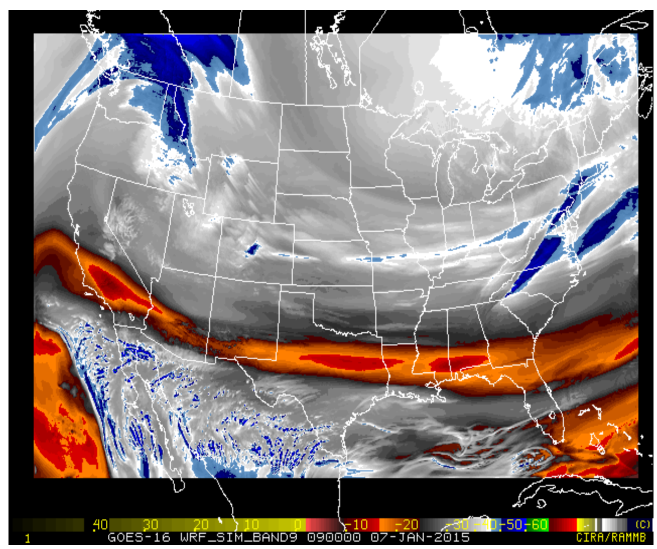

Figure 20. Forecast synthetic water vapor image (6.95 µm) from the 4-km NSSL WRF-ARW model from 0900 UTC 7 January 2015 closely resembles the observed *GOES* water vapor image across the SAMs shown in Fig. 18a. *Click image for an animation from 0900 to 2200 UTC.*

operational forecasts is also worthy of additional investigation. Verification of the accuracy of synthetic satellite imagery in orographic cirrus scenarios would also be helpful in determining to what extent the imagery can be incorporated into the forecast process.

Acknowledgments. The authors acknowledge Dr. David Radell, Brian Miretzky, Frank Alsheimer, and Bryan Jackson for their contributions and guidance during this experiment. We also acknowledge Chad Gravelle for providing the synthetic water vapor imagery example. Finally, we thank the reviewers for providing valuable feedback during the editing process. Reference to any specific commercial products, process, or service by trade name, trademark, manufacturer, or otherwise does not constitute or imply its recommendation or favoring by the United States Government or NOAA/National Weather Service. Use of information from this publication shall not be used for advertising or product endorsement purposes.

REFERENCES

Amante, C., and B. W. Eakins, 2009: ETOPO1 1 Arc-minute global relief model: Procedures, data sources and analysis. NOAA Technical Memorandum NESDIS NGDC-24. National Geophysical Data Center, NOAA. CrossRef.

AMS, cited 2015: Glossary of Meteorology. [Available online at glossary.ametsoc.org/wiki/Froude_number.]

Bikos, D., and Coauthors, 2012: Synthetic satellite imagery for real-time high-resolution model evaluation. *Wea. Forecasting*, **27**, 784–795, CrossRef.

Brown, P. R. A., 1983: Aircraft measurements of mountain waves and their associated momentum flux over the British Isles. *Quart. J. Roy. Meteor. Soc.*, **109**, 849–865, CrossRef.

Chevallier, F., and G. Kelly, 2002: Model clouds as seen from space: Comparison with geostationary imagery in the 11-µm window channel. *Mon. Wea. Rev*., **130**, 712–722, CrossRef.

____, P. Bauer, G. Kelly, C. Jakob, and T. McNally, 2001: Model clouds over oceans as seen from space: Comparison with HIRS/2 and MSU radiances. *J. Climate*, **14**, 4216–4229, CrossRef.

Conover, J. H., 1964: The identification and significance of orographically induced clouds observed by TIROS satellites. *J. Appl. Meteor.*, **3**, 226–234, CrossRef.

Dean, S. M., B. N. Lawrence., R. G. Grainger, and D. N. Heuff, 2005: Orographic cloud in a GCM: The missing cirrus. *Clim. Dyn.*, **24**, 771–780, CrossRef.

Durran, D. R., 1986: Another look at downslope windstorms. Part I: The development of analogs to supercritical flow in an infinitely deep, continuously stratified fluid. *J. Atmos. Sci.*, **43**, 2527–2543, CrossRef.

____, and J. B. Klemp, 1983: A compressible model for the simulation of moist mountain waves. *Mon. Wea. Rev.*, **111**, 2341–2361, CrossRef.

Ellrod, G. 1983: Orographic cirrus along the Appalachian Mountains. *U. S. Department of Commerce Satellite Applications Information Note.* **83/2**, 8C-1–8C-5. [Available from National Weather Service Forecast Office, 1005 Capability Drive, Suite 300, Raleigh, NC 27606.]

Grubišić, V., and B. J. Billings, 2008: Climatology of the Sierra Nevada mountain-wave events. *Mon. Wea. Rev.*, **136**, 757–768, CrossRef.

Hanson, T., M. Matthewson, T. J. LeFebvre, and M. Romberg, 2001: Forecast methodology using the GFE suite. Preprints, *17th Int. Conf. on Interactive Information and Processing Systems for Meteorology, Oceanography, and Hydrology*, Albuquerque, NM, Amer. Meteor. Soc., 1.13. [Available online at ams.confex.com/ams/annual2001/techprogram/paper_18722.htm.]

Henry, A. J., 1899: Wave or billow clouds. *Mon. Wea. Rev.*, **27**, 57–58, CrossRef.

Jiang, Q., and J. D. Doyle, 2006: Topographically generated cloud plumes. *Mon. Wea. Rev.*, **134**, 2108–2127, CrossRef.

____, and ____, 2008: On the diurnal variation of mountain waves. *J. Atmos. Sci.*, **65**, 1360–1377, CrossRef.

Kalnay, E., and Coauthors, 1996: The NCEP/NCAR 40-year reanalysis project. *Bull. Amer. Meteor. Soc.*, **77**, 437–471, CrossRef.

Lee, Y.-K., J. A. Otkin, and T. J. Greenwald, 2014: Evaluating the accuracy of a high-resolution model simulation through comparison with MODIS observations. *J. Appl. Meteor. Climatol.*, **53**, 1046–1058, CrossRef.

Lin, H., K. J. Noone, J. Ström, and A. J. Heymsfield, 1998: Dynamical influences on cirrus cloud formation process. *J. Atmos. Sci.*, **55**, 1940–1949, CrossRef.

Lindsay, C. V., 1962: Mountain waves in the Appalachians. *Mon. Wea. Rev.*, **90**, 271–276, CrossRef.

Parke, P. S., 1980: High attitude orographic clouds over southern Maine. *Natl. Wea. Dig.* **5**, 7–12. [Available online at www.nwas.org/digest/papers/1980/Vol05No2/1980v005no02-Parke.pdf.]

Otkin, J. A., and T. J. Greenwald, 2008: Comparison of WRF model-simulated and MODIS-derived cloud data. *Mon. Wea. Rev.*, **136**, 1957–1970, CrossRef.

Scorer, R. S., 1949: Theory of waves in the lee of mountains. *Quart. J. Roy. Meteor. Soc.*, **75,** 41–56, CrossRef.